Journal of Computational Physics 228 (2009) 717–730

Contents lists available at ScienceDirect

Journal of Computational Physics

journal homepage: www.elsevier.com/locate/jcp

Reconstruction of shapes and impedance functions using few far-field measurements

Lin He [a,*], Stefan Kindermann [b], Mourad Sini [c]

[a] Luminescent Technologies Inc., 2471 East Bayshore Road, Palo Alto, CA 94303, USA
[b] Industrial Mathematics Institute, Johannes Kepler University, Altenbergerstrasse 69, Linz, Austria
[c] RICAM, Altenbergerstrasse 69, Linz 4040, Austria

ARTICLE INFO

Article history:
Received 29 November 2007
Received in revised form 8 June 2008
Accepted 29 September 2008
Available online 18 October 2008

Keywords:
Inverse scattering
Far-field pattern data
Robin type boundary conditions
Boundary integral methods
Level set methods
Shape derivatives

ABSTRACT

We consider the reconstruction of complex obstacles from few far-field acoustic measurements. The complex obstacle is characterized by its shape and an impedance function distributed along its boundary through Robin type boundary conditions. This is done by minimizing an objective functional, which is the L^2 distance between the given far-field information g^∞ and the far-field of the scattered wave u^∞ corresponding to the computed shape and impedance function. We design an algorithm to update the shape and the impedance function alternatively along the descent direction of the objective functional. The derivative with respect to the shape or the impedance function involves solving the original Helmholtz problem and the corresponding adjoint problem, where boundary integral methods are used. Further we implement level set methods to update the shape of the obstacle. To combine level set methods and boundary integral methods we perform a parametrization step for a newly updated level set function. In addition since the computed shape derivative is defined only on the boundary of the obstacle, we extend the shape derivative to the whole domain by a linear transport equation. Finally, we demonstrate by numerical experiments that our algorithm reconstruct both shapes and impedance functions quite accurately for non-convex shape obstacles and constant or non-constant impedance functions. The algorithm is also shown to be robust with respect to the initial guess of the shape, the initial guess of the impedance function and even large percentage of noise.

1. Introduction

Let D be a bounded domain of $\mathbb{R}^2$ such that $\mathbb{R}^2 \setminus \overline{D}$ is connected. We assume that its boundary ∂D is of class C^2. The propagation of time-harmonic acoustic fields in homogeneous cylinder media can be modelled by the Helmholtz equation

$$\Delta u + \kappa^2 u = 0 \quad \text{in } \mathbb{R}^2 \setminus \overline{D}, \tag{1}$$

where $\kappa > 0$ is the wave number. At the obstacle boundary, ∂D, we assume that the total field u satisfies the Robin type boundary condition. That is,

$$\frac{\partial u}{\partial n} + i\kappa\sigma u = 0 \quad \text{on } \partial D \tag{2}$$

* Corresponding author.
E-mail addresses: lhe@luminescent.com, lin.he@ricam.oeaw.ac.at (L. He), kindermann@indmath.uni-linz.ac.at (S. Kindermann), mourad.sini@ricam.oeaw.ac.at (M. Sini).

0021-9991/$ - see front matter © 2008 Elsevier Inc. All rights reserved.
doi:10.1016/j.jcp.2008.09.029

with some impedance function σ where n is the outward unit normal of ∂D. We assume that σ is a real valued C^1-continuous function and has a uniform lower bound $\sigma_- > 0$ on ∂D. The boundary ∂D is referred to be coated.

For a given incident plane wave $u^i(x,d) = e^{i\kappa d\cdot x}$ with incident direction $d \in \mathbb{S}^1$, where $\mathbb{S}^1$ is the unit circle in $\mathbb{R}^2$, we look for a solution $u(x,d) := u^i(x,d) + u^s(x,d)$ of (1), (2), where the scattered field u^s satisfies the Sommerfeld radiation condition

$$\lim_{r\to\infty} \sqrt{r}\left(\frac{\partial u^s}{\partial r} - i\kappa u^s\right) = 0 \tag{3}$$

with $r = |x|$ and the limit is uniform for all directions $\hat{x} := x/|x| \in \mathbb{S}^1$. It is well known (cf. [7]) that the scattered wave has the asymptotic behavior:

$$u^s(x,d) = \frac{e^{i\kappa r}}{\sqrt{r}} u^\infty(\hat{x},d) + O(r^{-3/2}), \quad r \to \infty, \tag{4}$$

where the function $u^\infty(\hat{x},d)$ is called the far-field of the scattered wave $u^s(x,d)$ corresponding to the incident direction d.

The problem we are considering is formulated as the following inverse scattering problem.

Complex obstacles reconstruction problem. *Given* $u^\infty(\hat{x},d)$ for every $\hat{x} \in S^1$ *and for* K *incident directions* $d = d_1, d_2, \ldots, d_K$, *we want to reconstruct the complex obstacle* $(\partial D, \sigma)$.

In the case where d varies in a connected open subset of S^1, we have uniqueness of the inverse problem, see [19]. This uniqueness issue is largely open if we restrict ourselves to a finite number of incident directions. For some particular situations partial results are known. Indeed, in the case where the Robin boundary condition is replaced by the Dirichlet one (which is "similar" to take σ large in the Robin boundary condition), local uniqueness results for detecting the shapes are obtained, see [8,30,12] as well as local stability results, see [16,17,28]. These results are valid for small obstacles, see [8,16,17], and for close obstacles, see [30,12,28]. In addition, if we know an upper bound of the size of obstacles, then we can estimate the number of incident directions needed to insure uniqueness, see [8,12]. Moreover, if we know in advance that the obstacle D is polygonal, then two incident directions are enough for detecting $(\partial D, \sigma)$, see [21] and the references there, while for the Dirchlet case one incident direction is enough, see [1]. For this particular form of the obstacle, stability estimates are also provided in [25]. For general forms of obstacles and for Robin boundary conditions, the local uniqueness question is still an open issue. In case we know a-priori the obstacle, then a stability result for detecting the surface impedance is given in [29].

The object of this paper is to design a level set type [24] algorithm combined with boundary integral methods to reconstruct $(\partial D, \sigma)$ from few incident directions. Reconstructing shapes by level set methods, introduced by Santosa for inverse problems in [27], has a long history in both shape optimization and inverse scattering fields, see review papers [4,9] for more details. The level set method introduced by Osher and Sethian in [24] tracks the motion of an interface by embedding the interface as the zero level set of a signed distance function. The motion of the interface is matched with the evolution of the zero level set. Therefore, by working with a one dimension higher level set function it is not necessary to track the propagation of the interface, topological changes can occur in a natural manner, and the technique extends easily to three dimensions. However, in our framework of combining level set methods with boundary integral methods we need an explicit boundary representation of the zero level set from the given level set function. Therefore, we do not particularly benefit from level set methods. However, a main justification for the use of the level set method is the possibility of generalization. Note that a parametrization approach has been used in [32], where a Newton method was applied using the derivative with respect to the parametrization basis function. This might be more efficient, but the obvious drawback is the inherent need of a parametrization of the boundary, which requires some sort of a priori guess (such as the number of connected components) of the solution. On the contrary, in our approach the only need for a parametrization of the boundary comes from the computations of the forward problem, more precisely from the use of the boundary integral method for computing the far-field. A parametrization procedure for the inverse problem is not needed when the far-field is computed by finite element methods, for instance. Another possible application of the level set method are near-field problems (e.g. impedance tomography), where finite elements are a usual tool for approximation the forward problem. In these cases we can fully benefit from the advantages of a parametrization free algorithm for the inverse problems, in particularly by allowing topological changes. Therefore, the level set procedure can be applied to multi scattering problems as well. This will be our future work and is illustrated in more detail in Section 4.

Moreover, the novelty of our work lies in that we can reconstruct both the shape D and the impedance function $\sigma(x)$ by using the gradient descent method to minimize a least squares functional related with the given far-field data. To do so we need first to compute derivatives of the minimizing functional with respect to the shape and the impedance function, and then update the level set function via the shape derivative and update the impedance function via the impedance derivative alternatively. This is a non-convex problem and there is no uniqueness guaranteed. Nevertheless our numerical results surprisingly show very good reconstructions of both shapes and impedance functions, for non-convex shapes and non-constant impedance functions.

To find an explicit boundary curve of the zero level set from the given level set function, we have to assume that the obstacle is star-shape like and a point inside the obstacle is known. This is a rather weak assumption and it can be given naturally in some real cases that the location of the obstacle is known. It can also be obtained by other direct and non-iterative imaging methods, such as [15] which uses full far-field data and multiple frequencies to obtain accurate shape reconstructions, or [10] which uses topological derivatives to obtain rough shape reconstructions from full or partial far-field data,

or [23,20] which use full far-field data to reconstruct an approximation of the complex obstacle $(\partial D, \sigma)$. Particularly, we can further extend our work by using the reconstructions of the complex obstacle $(\partial D, \sigma)$ from [23,20] as the initial guess for the shape and the impedance function.

The rest of the paper is organized as follows. In Section 2 we propose to minimize a least squares functional and compute partial derivatives of this minimizing functional with respect to the shape and the impedance functional. In Section 3 we focus on how to solve the Helmholtz equation with the Robin type boundary condition and the Sommerfeld radiation condition by the boundary integral method, recognized as an efficient method in the classical scattering literature. We then describe in Section 4 the implementation of level set methods to reconstruct shape including some special treatments: a parametrization form of the zero level set from the given level set function and an extension of the computed shape derivative to the whole domain. Next section we deal with how to update the impedance function. We finally introduce our algorithm of reconstructing both the shape and the impedance function in Section 6 and we display numerical results from our algorithm in Section 7.

2. The minimization problem and the partial derivatives

As we mentioned, we are given the far-field patterns, $g_j^\infty(\hat{x}), j = 1, \ldots, K$, of the scattered waves $g_j^s(x)$, corresponding to the exact shape and the exact impedance function at an incident direction d_j, we want to reconstruct the shape of the obstacle and the surface impedance on the surface of the obstacle. To do so, we minimize the following least squares functional:

$$F(\partial D, \sigma) = \frac{1}{2}\sum_{j=1}^{K}\int_{\mathbb{S}^1} |u_j^\infty(\partial D, \sigma)(\hat{x}) - g_j^\infty(\hat{x})|^2 ds(\hat{x}), \tag{5}$$

where $u_j^\infty(\partial D, \sigma)(\hat{x})$ is the computed far-field pattern obtained from a shape D and an impedance function $\sigma(x)$ at the incident direction d_j. To calculate the derivative of this functional with respect to the shape or the impedance function, we first find the derivative of the far-field pattern $u_j^\infty(\partial D, \sigma)(\hat{x})$ with respect to the scattered wave $u_j^s(\partial D, \sigma)(x)$ and then calculate the derivative of $u_j^s(\partial D, \sigma)(x)$ with respect to the shape or the impedance function based on a variational formulation of the Helmholtz problem given in the next subsection.

To simplify the notation for the later computation, throughout the whole section, we omit the dependence on d_j and rewrite (5) as

$$F(\partial D, \sigma) = \frac{1}{2}\int_{\mathbb{S}^1} |u^\infty(\partial D, \sigma)(\hat{x}) - g(\hat{x})|^2 ds(\hat{x}). \tag{6}$$

In our numerical experiments, we computed (5) with four uniformly distributed incident waves. We can certainly use more than four incident waves and also for directions restricted to a limited angle (cf. [10]) (for example, $d_j \in [-\pi/4, \pi/4]$), however that is not the purpose of our paper. We are also aware of the approach of using a single incident wave but multiple frequencies to reconstruct the shape of the boundary (cf. [10,11]) but that is also out of the scope of our work.

2.1. The near-field–far-field map and the partial derivatives

We define a map from the scattered wave u^s to the far-field pattern u^∞ as

$$A : L^2(\partial D) \to L^2(\mathbb{S}^1): \quad u^s(\partial D, \sigma)(x)|_{\partial D} := f(x) \to u^\infty(\partial D, \sigma)(\hat{x}),$$

which is the Dirichlet–Laplace operator for the scattering problem. We know the explicit representation of A from [7] as

$$(Af)(\hat{x}) = (K^\infty - i\eta S^\infty)(I + K - i\eta S)^{-1} f, \tag{7}$$

where $\eta > 0$ is a constant, I is the identity operator, S and K are the single layer operator and the double layer operator respectively, and S^∞ and K^∞ are correspondingly the far-field counterpart of the single or double layer operator. For more information on these operators, we refer to Section 3 in [7].

Now, by denoting $u_{\partial D}^s$ and u_σ^s the partial derivatives of $u^s(\partial D, \sigma)$ with respect to ∂D and σ, respectively, we obtain the derivatives of the minimizing functional $F(\partial D, \sigma)$ from (6) with respect to ∂D and σ as follows:

$$\begin{aligned} F_{\partial D}(\partial D, \sigma) &= \mathrm{Re}\left[\int_{\mathbb{S}^1} (Au_{\partial D}^s)(\hat{x})\overline{u^\infty(\partial D, \sigma)(\hat{x}) - g(\hat{x})} ds(\hat{x})\right] \\ &= \mathrm{Re}\left[\int_{\partial D} u_{\partial D}^s(x)\overline{(A^*(u^\infty(\partial D, \sigma) - g))(x)} ds(x)\right] \end{aligned}$$

and

$$\begin{aligned} F_\sigma(\partial D, \sigma) &= \mathrm{Re}\left[\int_{\mathbb{S}^1} (Au_\sigma^s)(\hat{x})\overline{u^\infty(\partial D, \sigma)(\hat{x}) - g(\hat{x})} ds(\hat{x})\right] \\ &= \mathrm{Re}\left[\int_{\partial D} u_\sigma^s(x)\overline{(A^*(u^\infty(\partial D, \sigma) - g))(x)} ds(x)\right], \end{aligned}$$

where $A^* : L^2(\mathbb{S}^1) \to L^2(\partial D)$ is the adjoint operator of A. We define

$$\gamma(x) := (A^*(u^\infty(\partial D, \sigma) - g))(x),$$

then the above equations become

$$F_{\partial D}(\partial D, \sigma) = \mathrm{Re}\left[\int_{\partial D} u^s_{\partial D}(x)\overline{\gamma(x)}ds(x)\right] \tag{8}$$

and

$$F_{\sigma}(\partial D, \sigma) = \mathrm{Re}\left[\int_{\partial D} u^s_{\sigma}(x)\overline{\gamma(x)}ds(x)\right]. \tag{9}$$

Therefore, to compute derivatives of F with respect to the shape and the impedance function, we need to compute $\overline{\gamma(x)}$, $u^s_{\partial D}(x)$ and $u^s_{\sigma}(x)$. However, as presented later, we do not compute the derivatives $u^s_{\partial D}(x)$ and $u^s_{\sigma}(x)$ directly. Instead we use a variational formulation and its adjoint problem to transform (8) and (9) into some boundary integrals, which are only related with the solutions of the original Helmholtz problem and its adjoint problem.

Remark 2.1. Here we use the notation of the partial derivatives $u^s_{\partial D}(x)$ and $u^s_{\sigma}(x)$ before we validate the existence of the both derivatives, which will be given in Section 2.3.

Remark 2.2. In the case where κ^2 is not an eigenvalue for the Dirichlet-Laplace operator on D we can let $\eta = 0$ from (7) and then we obtain Af as

$$Af = K^\infty(I + K)^{-1}f,$$

see [6]. This is a reasonable assumption since the set of eigenvalues of Dirichlet–Laplacian operator on D is discrete.

2.2. A variational form for the scattering problem

Let Ω_R be a large ball, with radius R, containing strictly D. We follow the ideas in [11]. From [11,18], we know that the solution $u := u^i + u^s$ of (1)–(3) satisfies

$$\begin{cases} \Delta u + \kappa^2 u = 0 & \text{in } \Omega_R \setminus \overline{D}, \\ \frac{\partial u}{\partial n} + i\kappa\sigma u = 0 & \text{on } \partial D, \\ \frac{\partial u_s}{\partial n} = M(u_s) & \text{on } \partial\Omega_R, \end{cases} \tag{10}$$

where

$$M(u) := \sum_{l=-\infty}^{\infty} z_{|l|}(\kappa, R)\psi_l(x)\int_{\partial\Omega_R}\overline{\psi_l}(y)u(y)ds(y)$$

with $\psi_l(x) := \sqrt{\frac{1}{2\pi R}}e^{il\theta}$, for $x = R(\cos(\theta), \sin(\theta)) \in \partial\Omega_R$ and $z_{|l|}(\kappa, R) := \frac{\kappa H^{(1)\prime}_{|l|}(\kappa R)}{H^{(1)}_{|l|}(\kappa R)}$, $H^{(1)}_{|l|}$ is the Hankel function of first kind of order l and $H^{(1)\prime}_{|l|}$ is its derivative.

Conversely, if $u_{\Omega_R} := u^i + u^s_{\Omega_R}$ satisfies (10), then we can extend $u^s_{\Omega_R}$ (and then u_{Ω_R}) to $\mathbb{R}^2 \setminus \overline{D}$ by solving the Dirichlet exterior problem

$$\begin{cases} \Delta u^e + \kappa^2 u^e = 0 & \text{in } \mathbb{R}^2 \setminus \overline{\Omega_R}, \\ u^e = u^s_{\Omega_R} & \text{on } \partial\Omega_R, \\ \lim\limits_{r\to\infty}\sqrt{r}\left(\frac{\partial u^e}{\partial r} - i\kappa u^e\right) = 0. \end{cases}$$

Thus the function u defined by $u := u_{\Omega_R}$ on $\Omega_R \setminus \overline{D}$ and $u := u^i + u^e$ on $\mathbb{R}^2 \setminus \overline{\Omega_R}$ satisfies (1)–(3). This shows that the problem (1)–(3) and the problem (10) are equivalent.

The variational form of the problem (10) is given by

$$\int_{\Omega_R\setminus\overline{D}}(-\nabla u \cdot \overline{\nabla v} + \kappa^2 u\bar{v})dx + i\kappa\int_{\partial D}\sigma u\bar{v}\,ds(x) + \int_{\partial\Omega_R}M(u)\bar{v}\,ds(x) = \int_{\partial\Omega_R}(M(u^i) - \frac{\partial u^i}{\partial n})\bar{v}\,ds(x) \tag{11}$$

for u, v both in $H^1(\Omega \setminus \overline{D})$.

2.3. The partial derivative of $F(\partial D, \sigma)$ w.r.t. the shape

To calculate the derivative of the minimizing functional $F(\partial D, \sigma)$ with respect to the shape ∂D for a fixed impedance function $\sigma(x)$, we need a formal definition of shape derivatives. In the framework of Murat–Simon [22,31], it is defined as the following. Let $D \subset \Omega \subset R^N$ be a reference domain. Consider the perturbation under the map $\theta \in W^{1,\infty}(R^N, R^N)$, s.t. $\|\theta\|_{W^{1,\infty}} < 1$:

$$D_\theta = (I + \theta)D,$$

where I is the identity map. The set D_θ is defined as

$$D_\theta = \{x + \theta(x) \mid x \in D\}.$$

The shape derivative of an objective shape functional, $\mathscr{F} : \mathscr{R}^{\mathscr{N}} \to \mathscr{R}$, at D is defined as the Frechet differential of $\theta \to \mathscr{F}(\mathscr{D}_\theta)$ at 0 where θ can be viewed as a vector field advecting the reference domain Ω. The shape derivative $d_S\mathscr{F}(\mathscr{D})(\theta)$ depends only on $\theta \cdot n$ on the boundary ∂D because the shape of D does not change at all if θ is lying on the tangential direction of the domain D.

For an objective functional that is the integral on the volume of D or along the boundary of D, the following formulas can be easily obtained. If D is a smooth bounded open set, $f(x) \in W^{1,1}(R^N)$, and

$$\mathscr{F}(D) = \int_D f(x)dx,$$

the shape derivative is

$$d_S\mathscr{F}(D)(\theta) = \int_D \nabla \cdot (\theta(x)f(x)) = \int_{\partial D} \theta(x) \cdot n(x)f(x)ds(x). \tag{12}$$

If D is a smooth bounded open set, $f(x) \in W^{2,1}(R^N)$, and

$$\mathscr{F}(D) = \int_{\partial D} f(x)dx,$$

the shape derivative is

$$d_S\mathscr{F}(D)(\theta) = \int_{\partial D} \theta(x) \cdot n(x)\left(\frac{\partial f}{\partial n} + Hf\right)ds(x), \tag{13}$$

where H is the mean curvature of ∂D defined by $H = \nabla \cdot n$. These two formulas indicate that the shape derivative depends only on the boundary when the objective functional is a volume integral and the curvature plays a role when the objective functional is a surface integral.

Now, we are ready to calculate the derivative of u^s with respect to ∂D under a perturbation map $V(x) \in W^{1,\infty}(R^2, R^2)$. With $D_t := (I + tV(x))D$ denoting the perturbed shape, u_t denoting the solution of (11) when replacing D by D_t, and $u^s_{\partial D} = u_{\partial D} = \lim_{t\to 0}\frac{1}{t}(u_t - u)$ denoting the partial derivative of u^s with respect to the shape, we derive below to obtain the derivative $F_{\partial D}(\partial D, \sigma)$. Based on the shape derivative formulas above (12) and (13), we subtract the two variational formulations for u_t and u, divide it by t and take the zero limit of t, then we end up to have

$$\begin{aligned}&\Big(-\textstyle\int_{\Omega_R\setminus\overline{D}} \nabla u_{\partial D}\overline{\nabla v}\,dx + \int_{\partial D}(V.n)\nabla u\overline{\nabla v}ds(x)\Big) + \kappa^2\Big(\int_{\Omega_R\setminus\overline{D}} u_{\partial D}\bar{v}\,dx - \int_{\partial D}(V.n)u\bar{v}\,ds(x)\Big)\\ &+i\kappa\Big(\textstyle\int_{\partial D}\sigma u_{\partial D}\bar{v}\,ds(x) + \int_{\partial D}(V.n)(\frac{\partial(\sigma u\bar{v})}{\partial n} + \nabla\cdot n(\sigma u\bar{v}))ds(x)\Big) + \int_{\partial\Omega_R} M(u_{\partial D})\bar{v}\,ds(x) = 0.\end{aligned}$$

We rearrange the above equation and get

$$\begin{aligned}&-\textstyle\int_{\Omega_R\setminus\overline{D}} \nabla u_{\partial D}\overline{\nabla v}\,dx + \kappa^2\int_{\Omega_R\setminus\overline{D}} u_{\partial D}\bar{v}\,dx + i\kappa\int_{\partial D}\sigma u_{\partial D}\bar{v}\,ds(x) + \int_{\partial\Omega_R} M(u_{\partial D})\bar{v}\,ds(x)\\ &+\textstyle\int_{\partial D}(V.n)\Big\{\nabla u\overline{\nabla v} - \kappa^2 u\bar{v} + i\kappa\frac{\partial(\sigma u\bar{v})}{\partial n} + i\kappa(\nabla\cdot n)(\sigma u\bar{v})\Big\}ds(x) = 0.\end{aligned} \tag{14}$$

By the solvability of the above equation (14), we know that the partial derivative of u^s with respect to ∂D under a perturbation V exists. Similar can be said about the existence of u^s_σ.

Now, we denote w as the solution of the adjoint problem

$$-\int_{\Omega_R\setminus\overline{D}} \nabla w\overline{\nabla v}dx + \kappa^2\int_{\Omega_R\setminus\overline{D}} w\bar{v}\,dx - i\kappa\int_{\partial D}\sigma w\bar{v}\,ds(x) + \int_{\partial\Omega_R} w\overline{M(v)}ds(x) = \int_{\partial D}\gamma(x)\bar{v}\,ds(x),$$

$\forall v \in H^1(\Omega_R \setminus \overline{D})$. By taking the conjugate of the above equation, we have:

$$-\int_{\Omega_R\setminus\overline{D}} \overline{\nabla w}\nabla v\,dx + \kappa^2\int_{\Omega_R\setminus\overline{D}} \bar{w}v\,dx + i\kappa\int_{\partial D}\sigma\bar{w}v\,ds(x) + \int_{\partial\Omega_R}\bar{w}M(v)ds(x) = \int_{\partial D}\overline{\gamma(x)}v\,ds(x). \tag{15}$$

Since $\overline{M^*(w)} = M(\bar{w})$, we have

$$\int_{\partial\Omega_R} M(v)\bar{w}\,ds(x) = \int_{\partial\Omega_R} v\overline{M^*(w)}ds(x) = \int_{\partial\Omega_R} vM(\bar{w})ds(x).$$

We plug it in (15) and replace v by $\bar{v}$ to get

$$-\int_{\Omega_R\setminus\overline{D}} \overline{\nabla w\nabla v}\,dx + \kappa^2\int_{\Omega_R\setminus\overline{D}} \bar{w}\bar{v}\,dx + i\kappa\int_{\partial D}\sigma\bar{w}\bar{v}\,ds(x) + \int_{\partial\Omega_R} M(\bar{w})\bar{v}\,ds(x) = \int_{\partial D}\overline{\gamma(x)}\bar{v}\,ds(x).$$

This is equivalent to say that $\bar{w}$ is the restriction to $\Omega_R \setminus \overline{D}$ of the solution of the scattering problem:

$$\begin{cases} \Delta\tilde{w} + \kappa^2\tilde{w} = 0 \quad \text{in } \mathbb{R}^2 \setminus \overline{D}, \\ \frac{\partial\tilde{w}}{\partial n} + i\kappa\sigma\tilde{w} = \overline{\gamma(x)} \quad \text{on } \partial D, \\ \lim_{r\to\infty} \sqrt{r}(\frac{\partial\tilde{w}}{\partial r} - i\kappa\tilde{w}) = 0. \end{cases} \tag{16}$$

Replacing v by $u_{\partial D}$ in (15), we get

$$\begin{aligned} F_{\partial D}(\partial D, \sigma) &= \mathrm{Re}\left[\int_{\partial D} \overline{\gamma(x)} u_{\partial D}\, ds(x)\right] \\ &= \mathrm{Re}\left[-\int_{\Omega_R\setminus\overline{D}} \nabla\bar{w}\nabla u_{\partial D}\, dx + \kappa^2 \int_{\Omega_R\setminus\overline{D}} \bar{w} u_{\partial D}\, dx + i\kappa \int_{\partial D} \sigma\bar{w} u_{\partial D}\, ds(x) + \int_{\partial\Omega_R} M(u_{\partial D})\bar{w}\, ds(x)\right]. \end{aligned} \tag{17}$$

Replacing v by w in (14), denoting

$$W := \left\{\nabla u\overline{\nabla w} + (-\kappa^2 + i\kappa\sigma(\nabla.n))u\bar{w} + i\kappa\frac{\partial(\sigma u\bar{w})}{\partial n}\right\} \tag{18}$$

and using (17), we have the shape derivative of the least squares functional $F(\partial D, \sigma)$ under the map $V(x)$ as

$$F_{\partial D}(\partial D, \sigma)(V) = -\mathrm{Re}\left[\int_{\partial D} (V.n) W\, ds(x)\right]. \tag{19}$$

It shows again that the shape derivative of $F(\partial D, \sigma)$ depends only on the boundary by normal projection of the velocity V and W, which is determined by u, w, ∇u and ∇w.

Remark 2.3. We can also use the Lagrange multiplier method to compute shape derivatives like it was done in [2,11].

2.4. The partial derivative of $F(\partial D, \sigma)$ w.r.t. the impedance function

Now we compute the derivative of the least squares $F(\partial D, \sigma)$ with respect to σ when D is fixed. We try to find the Frechet derivative of u with respect to σ in the direction of $h(x) : \mathbb{R}^2 \to R$. This is very similar to the procedure of obtaining the shape derivative: with the Frechet derivative $u_\sigma := \lim_{\epsilon\to 0} \frac{1}{\epsilon}(u(\sigma + \epsilon h) - u(\sigma))$, we take the difference between the two variational formulations, and let ϵ go to 0 to get:

$$\int_{\Omega_R\setminus\overline{D}} (-\nabla u_\sigma \cdot \overline{\nabla v} + \kappa^2 u_\sigma \bar{v}) dx + i\kappa \int_{\partial D} \sigma u_\sigma \bar{v}\, ds(x) + \int_{\partial\Omega_R} M(u_\sigma)\bar{v}\, ds(x) + i\kappa \int_{\partial D} hu\bar{v}\, ds(x) = 0. \tag{20}$$

Note that this equation is similar to the shape derivative equation (14) except that the term $i\kappa\int_{\partial D} hu\bar{v}\, ds(x)$ is replaced by $\int_{\partial D} V.nW\, ds(x)$ in (14). Therefore, with the same procedure including the same adjoint equation, we obtain the derivative of $F(\partial D, \sigma)$ with respect to σ

$$F_\sigma(\partial D, \sigma) = -\mathrm{Re}\left[i\kappa \int_{\partial D} hu\bar{w}\, ds(x)\right].$$

If we assume that σ is a real function, then we have

$$F_\sigma(\partial D, \sigma)(h) = \int_{\partial D} h\mathrm{Im}(\kappa u\bar{w}) ds(x). \tag{21}$$

Therefore, the derivative of $F(\partial D, \sigma)$ with respect to $\sigma(x)$ can be solely determined from u and w.

3. The solution of the scattering problem

In this work we resort to boundary integral methods to solve the Helmholtz problem (10) and the adjoint problem (16) due to the efficiency and rapid convergence of the method. Since the incident wave u^i is explicitly known it is enough to solve the scattered wave u^s from the following scattering problem:

$$\begin{cases} \Delta u^s + \kappa^2 u^s = 0, \quad \text{in } \Omega \setminus \overline{D}, \\ \frac{\partial u^s}{\partial \nu} + i\kappa\sigma u^s = f \quad \text{on } \partial D, \\ \frac{\partial u^s}{\partial \nu} = M[u^s] \quad \text{on } \partial\Omega_R, \end{cases} \tag{22}$$

where $f = -i\kappa e^{i\kappa d\cdot x}(d\cdot n + \sigma)$ in (10) and $f = \overline{\gamma(x)}$ in (16). Assuming that ∂D has an analytic expression, we can solve the scattering problem (22) based on potential method elaborated in the following proposition.

Proposition 3.1. *Let $\psi(x) \in C^{0,\alpha}(\partial D)$ be the unique solution of the following integral equation:*

$$(I - (K' + i\kappa\sigma S))\psi(x) = -2f(x), \tag{23}$$

then

1. *the solution to the scattering problem (22)* $u^s(x) \in C^{1,\alpha}(\Omega \setminus D)$ *is given by*

$$u^s(x) = \frac{1}{2}(S\psi)(x) = \int_{\partial D} \Phi(x,y)\psi(y)ds(y)$$

and

2. *the gradient of* $u^s(x)$ *is in* $C^{0,\alpha}(\Omega \setminus D)$ *with*

$$\nabla u^s(x) = \int_{\partial D} \nabla_x \Phi(x,y)\psi(y)ds(y) - \frac{1}{2}\psi(x)n(x) \quad \text{for } x \in \partial D.$$

Furthermore, the far-field pattern can be written as

3. $u^\infty(\hat{x}) = \frac{1}{2}S^\infty(\psi)(\hat{x}) = \int_{\partial D} \Phi^\infty(\hat{x},y)\psi(y)ds(y)$ *for* $x \in \partial D$.

The proof of the points 1 and 3 of Proposition 3.1 can be given as in Section 3.2 of [7] while the point 2 is justified by Theorem 2.17 of [6], assuming that κ^2 is not a Dirichlet–Laplacian eigenvalue in D.

4. The reconstruction of the shape by implementing the level set method

The level set method [24], a well-known implicit boundary representation method, is applied to reconstruct the boundary of the obstacle by representing the interface ∂D as the zero level set of a time dependent signed distance function $\phi(x,t)$

$$\phi(x,t)\begin{cases} < 0 & x \in D \\ > 0 & x \in \mathbb{R}^2 \setminus \overline{D}. \end{cases}$$

The motion of the interface is matched with the evolution of the zero level set, and the resulting partial differential equation for the evolution of the level set function resembles a Hamilton–Jacobi equation. To do so, we take the derivative of $\phi(x(t),t) = 0$ for $x(t) \in \partial D$ with respect to t and we obtain

$$\phi_t + x'(t) \cdot \nabla\phi = 0.$$

To minimize the energy functional $F(\partial D, \sigma)$ for a fixed impedance function $\sigma(x)$, we choose a descent direction $x\prime(t) := V = Wn = W\frac{\nabla\phi}{|\nabla\phi|}$, then the above equation becomes

$$\phi_t + W|\nabla\phi| = 0. \tag{24}$$

Therefore, to update the level set function $\phi(x,t)$, we need to compute the velocity W from (18) by obtaining the solutions of the Helmoltz problem (10) and the adjoint problem (16) from Proposition 3.1. To calculate the boundary integrals, we need to find a parametrization form of the zero level set for a given level set function. The details of this parametrization will be given in Section 4.2, but here we mention that we are aware of the limitation of our algorithm as trying to combine these two methods. The drawback is that the boundary has to be a starlike shape and the change of topology of our level set function is not allowed. From this sense, the use of level set methods is not necessary. For example, we can represent the boundary explicitly by some basis functions(trigonometric series, polynomials, etc.), and use the velocity W to update the boundary along the normal direction with an appropriate step size, this is introduced as the *Steepest Descent Approach* in [13]. This approach is rather inefficient in terms of computation time since for every time step size the resulting boundary has to be tested for admissibility and the both problems (Helmholtz and adjoint) have to be solved for the test of admissibility. For more details, we refer to [13]. Nevertheless, we justify the use of level set methods for the following three reasons:

- The level set method is more efficient since the choice of time step size for the Hamilton–Jacobi equation (24) is governed by the CFL condition.
- The computation time of updating the level set equation (24) or obtaining an explicit curve from a given level set function is relatively small compared with solving the linear equation (23) to obtain the density function $\psi(x)$. Therefore, we can afford to use a fine grid level set function for the accuracy of the boundary integral method. The details will be discussed more in the numerical results section.
- In a future work, we plan to compute the solutions of the Helmholtz problem (10) and the adjoint problem (16) by solving the variational problem (11) through finite element methods. To solve (11), we propose to approximate the second term in (11), a boundary integral on ∂D, by the use of delta function of the level set function $\phi(x,t)$ to avoid the necessity of an explicit boundary representation. In such a way topology changes can occur naturally to the level set method, such as two objects merging into one or one object splitting to two. Therefore, it can be applied to multi scattering problems.

Finally, before we present our algorithm of reconstructing the shape by combining the level set method and the boundary integral method, we note that W is only defined on the boundary of the obstacle ∂D. Therefore, to update the level set function $\phi(x)$ defined on the whole domain, we need to extend W to the whole domain. This will be elaborated in Section 4.3.

4.1. Our algorithm to reconstruct the shape when the impedance function is known

1. The 0th iteration: given an initial level set function $\phi^0(x)$, with parametrization, we obtain the boundary of the obstacle represented by $\partial D^0 = \{x : x \in \mathbb{R}^2, \phi^0(x) = 0\}$. From Proposition 3.1 we obtain $u^\infty(\partial D^0, \sigma)(x)$ to compute the energy functional $F(\partial D^0, \sigma)$.
2. The nth iteration ($n > 0$): based on Proposition 3.1 and with the given ∂D^{n-1} we obtain the solutions of the Helmholtz problem (10) and the adjoint problem (16) u and $\bar{w}$, as well as ∇u and $\nabla \bar{w}$.
3. Through (18) we obtain a velocity W defined only on ∂D^{n-1}. We extend the velocity W by a linear transport equation described by (25) in Section 4.3 and plug it in (24), then we obtain an updated level set function $\phi^n(x)$.
4. We re-initialize (cf. [26]) the level set function $\phi^n(x)$ every five iterations.
5. With the newly updated level set function $\phi^n(x)$, we perform parametrization to obtain the boundary of the obstacle ∂D^n. We calculate $u^\infty(\partial D^n, \sigma)(x)$ and then the energy functional $F(\partial D^n, \sigma)$. We compare this new energy with the previous one $F(\partial D^{n-1}, \sigma)$. If a stopping criterion is satisfied, we stop here.
6. Otherwise we move on to the $(n+1)$th iteration by going back to the second step.

4.2. Parametrization

To find a parametrization of the zero level set from a level set function $\phi^n(x)$, as we mentioned in the introduction we assume that a point $z = (x_1, x_2)$ inside the exact obstacle is known. Therefore, starting from an initial level set function $\phi^0(x)$ with $\phi^0(z) < 0$, we will have $\phi^n(z) < 0\ \forall n > 0$. This is because if at the nth iteration $\phi^n(z) > 0$, then the reconstructed object is empty. But as we know, the least squares functional $F(\emptyset, \sigma)$ at the nth iteration is larger than the 0th iteration $F(\partial D^0, \sigma)$, which contradicts our minimizing algorithm. We approximate the zero level set by M uniformly distributed points. Naturally we start from (x_1, x_2), go along each radial line with an angle $\theta = 0, 2\pi/M, \ldots, 2\pi(M-1)/M$ and check the sign of the level set function for each grid lying on the radial line. Once the sign of the level set function for some grid becomes positive, then we can obtain a boundary point $(x_1(\theta), x_2(\theta))$ by a simple linear interpolation.

After we have M uniformly distributed points on the boundary of the obstacle, we use the Fourier series theory to find an analytical expression of the boundary of the obstacle ∂D^n. The analytical expression of ∂D^n is needed in the computation of scattering operators.

4.3. Velocity extension

At the nth iteration, with the given computed velocity W, we first obtain a preliminary extension V_0^n of W by extending W radial symmetrically from a point inside the obstacle. Here we choose $z = (x_1, x_2)$, the base point for the parametrization. Now with V_0^n and the level set function $\phi^n(x)$ we perform several (around 10) iterations of the following linear transport equation [4]

$$\frac{\partial w}{\partial t} + \operatorname{sign}(V_0^n)(\nabla w \cdot \nabla \phi^n) = 0 \tag{25}$$

to smooth the preliminary extension along the level sets of $\phi^n(x)$. We start from $w(t=0) = V_0^n$.

5. The reconstruction of the impedance function

Based on (21), the σ derivative of $F(\partial D, \sigma)$ for fixed shapes, it is natural to update the impedance function $\sigma(x)$ by the method of steepest descent. From now on, we define $\sigma(x)$ only on the boundary of obstacle ∂D, in terms of θ which is the angle of the point x to the center z from above. Particularly $\theta = 0, 2\pi/M, \ldots, 2\pi * (M-1)/M$ in our numerical experiments. In such a way, when the shape ∂D^{n-1} is updated to a new shape ∂D^n, $\sigma^{n-1}(x)$ is projected onto the new boundary ∂D^n by the use of angular coordinates. This new projected impedance function on ∂D^n, denoted as $\sigma^{n,0}(x)$, serves as the old $\sigma^{n-1}(x)$ to be updated in the minimization of $\sigma(x)$. See step 6 of our algorithm in the next section.

In addition, to prevent the reconstructed impedance function from being noisy, we add a regularization term

$$\frac{\lambda}{2}\int_{\partial D} |\nabla \sigma(x)|^2 ds(x)$$

to the least squares functional $F(\partial D, \sigma)$. The function of this regularization term is in favor of a smooth impedance function. A large λ tends to make a flat impedance function σ, i.e. $\sigma(x) \equiv const$. Thus if we have a priori information of the impedance function we can choose a proper regularization parameter λ.

Therefore, we end up updating $\sigma(x)$ by the following equation:

$$\sigma_t = \lambda \Delta \sigma - \kappa \operatorname{Im}(u\bar{w}). \tag{26}$$

Remark 5.1. In our algorithm, we do not use a regularization for the shape function. However, this can easily be included by adding a e.g. curvature term in the level set iteration. Note that even without regularization the level set iteration can be

viewed as an iterative regularization [5], if a stopping criteria is used. Also, the reinitialization procedure helps stabilizing the shapes during the iterations. In our numerical examples, we observed that an explicit regularization term was not necessary.

6. Our algorithm to reconstruct the shape and the impedance function

When both of the shape and the surface impedance function are unknown, we follow the algorithm described in Section 4.1 with an additional procedure to update $\sigma(x)$, which is described below:

1. The 0th iteration: given an initial level set function $\phi^0(x)$ and an initial impedance function $\sigma^0(x)$, with parametrization we first obtain the boundary of the obstacle ∂D^0 and then we compute the energy functional $F(\partial D^0, \sigma^0)$.
2. The nth iteration ($n > 0$): we set two indexes for ϕ and σ: $I_\phi = 1$ and $I_\sigma = 1$. With the given ∂D^{n-1} and $\sigma^{n-1}(x)$, we obtain u, ∇u, $\bar{w}$ and $\nabla \bar{w}$ from Proposition 3.1.

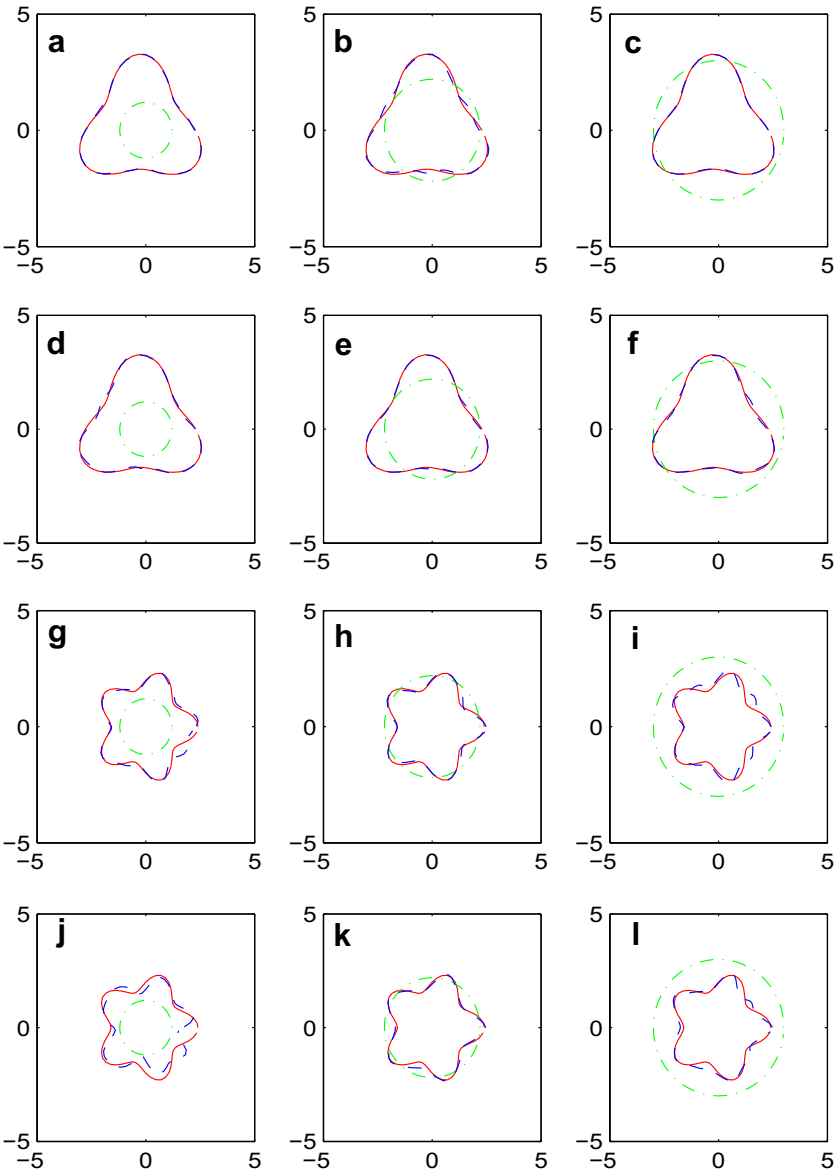

Fig. 1. First row: star shape, $\sigma(x) = 1$; second row: star shape, $\sigma(x) = \frac{2+\sin\theta\cos\theta}{(3+\sin\theta)^2}$; third row: leaf shape, $\sigma(x) = 1$; fourth row: leaf shape, $\sigma(x) = \frac{2+\sin\theta\cos\theta}{(3+\sin\theta)^2}$. First column: initial guess of $r = 1.2$; second column: $r = 2.2$; Third column: $r = 3.0$.

3. By simple calculation we obtain a velocity W defined only on ∂D^{n-1} from (18). Extending the velocity W to the whole domain and plug it in (24), we obtain a updated level set function $\phi^n(x)$.
4. We re-initialize (cf. [26]) the level set function $\phi^n(x)$ every five iterations.
5. With the newly updated level set function $\phi^n(x)$, we perform parametrization to obtain the boundary of the obstacle ∂D^n. We compute the energy functional $F(\partial D^n, \sigma^{n-1})$. We compare this new energy with the previous one $F(\partial D^{n-1}, \sigma^{n-1})$. If a stopping criterion is satisfied, we denote the index for the level set function $I_\phi = 0$.
6. The kth inner iteration ($k > 0$ and $k \leqslant m$) for updating $\sigma(x)$: with the new ∂D^n and $\sigma^{n,0}(x)$ (the latter is projected onto the new boundary ∂D^n by the old impedance function $\sigma^{n-1}(x)$), we solve the equivalent Helmholtz problem (10) and the adjoint problem (16) to obtain u and $\bar{w}$. We calculate the velocity $-\mathrm{Im}(\kappa u \bar{w})$ to obtain $\sigma^{n,k}(x)$ from (26).
7. With the fixed ∂D^n and the newly updated $\sigma^{n,k}(x)$, we compute the energy functional $F(\partial D^n, \sigma^{n,k})$. We compare this new energy with the previous one $F(\partial D^n, \sigma^{n,k-1})$. If $k < m$ and a stopping criterion is not satisfied, we go back to the sixth step to perform $(k+1)$th inner iteration for $\sigma(x)$. Otherwise, we denote the index for updating the impedance function $I_\sigma = 0$. If both indexes are zero, we stop here. Otherwise,
8. We move on to the $(n+1)$th outer iteration by going back to the second step.

Due to the stopping criterion, the number of iterations to update $\phi(x)$ and $\sigma(x)$ is not uniformly distributed like what we want: every iteration of updating $\phi(x)$ for m iterations of updating $\sigma(x)$. Therefore, we try to choose m to uniformly distribute the number of iterations to update the shape with a fixed impedance function and the number of iterations to update the impedance function with a fixed shape. For example, we perform two inner iterations of $\sigma(x)$ per iteration of $\phi(x)$ for all three reconstructions in Fig. 2, one iteration of $\sigma(x)$ per 10 iterations of $\phi(x)$ for the first two reconstructions in Fig. 3 and one iteration of $\sigma(x)$ per iteration of $\phi(x)$ for the third reconstruction in Fig. 3. Nevertheless in Fig. 4 we show that our reconstructions are relatively stable with respect to the choice of this number of inner iterations for updating $\sigma(x)$ per iteration of $\phi(x)$ or vice versa.

7. Numerical results

We consider the problem of identifying the shape and the impedance function of an impenetrable obstacle from the knowledge of its far-field scattering pattern obtained in response to four plane waves incident at angles 0, $\frac{\pi}{2}$, π and $\frac{3\pi}{2}$ and at a fixed frequency with the wave number $\kappa = 0.6$. The far-field pattern information is given at 64 uniformly distributed angles $0, 2\pi/64, \ldots, 2\pi * 63/64$. So is the parametrization with the base point z, which is chosen as $(-0.25, 0.2)$ for a star shape with polar coordinates (r, θ) where $r^2 + 1.2rsin(3\theta) = 2.4^2$ (cf. [3]) and $(0,0)$ for a shape of five leaves with $r = 2(1 + 0.2\cos(5\theta))$ (cf. [14]). Our numerical results are not sensitive to the choice of this point as long as it is inside the obstacle and not too close to the boundary of the obstacle. The impedance function $\sigma(x)$ (cf. [20]) is either a constant $\sigma(x) = 1$ or a smooth function $\sigma(x) = \frac{2+sin\theta\cos\theta}{(3+sin\theta)^2}$, where θ is the angle of the point $x \in \partial D$. The computing domain is $[-5,5] \times [-5,5]$ and the grid size for the level set method is $dx = dy = 10/64$. So the average number of grids per wave length is about 60, which is high compared with 30 from [11]. However, the computation time $O(64^2)$ for updating the level set

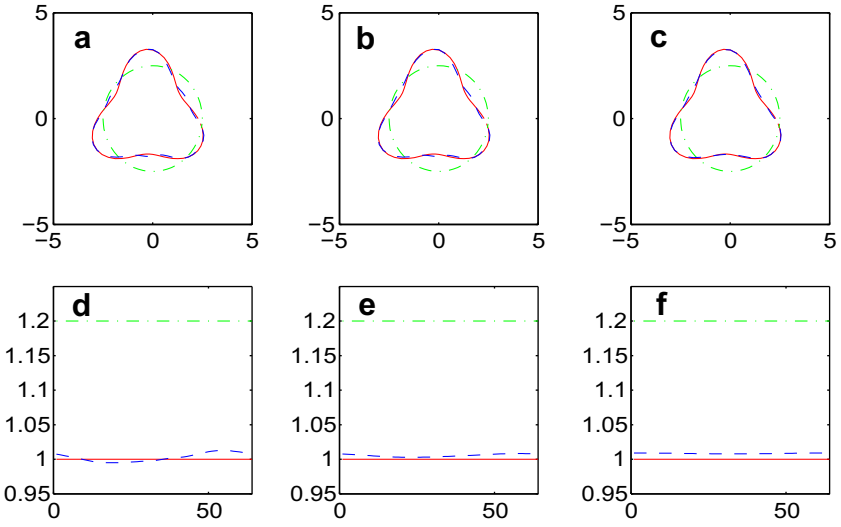

Fig. 2. First row: reconstructions of the shape; second row: reconstructions of the impedance function; first column: the regularization parameter $\lambda = 1$; Second column: $\lambda = 10$; third column: $\lambda = 100$.

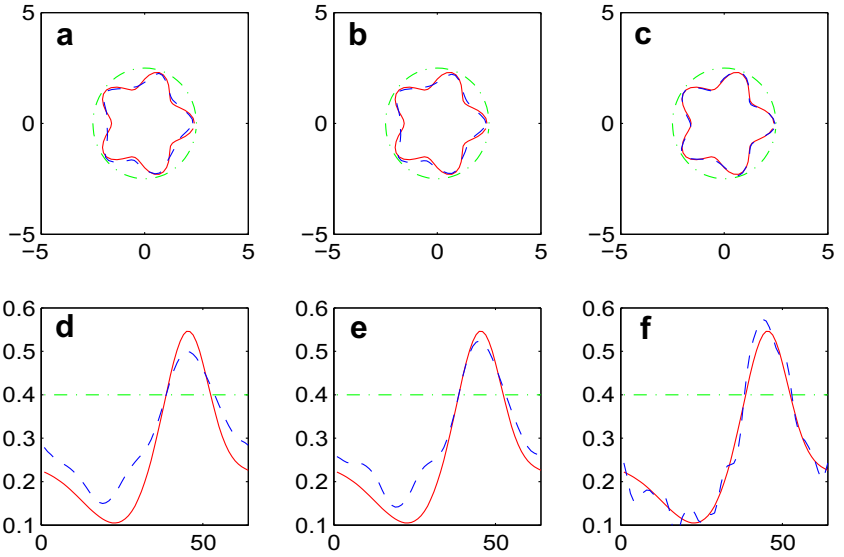

Fig. 3. First row: reconstructions of the shape; second row: reconstructions of the impedance function; first column: the regularization parameter $\lambda = 1$; second column: $\lambda = 0.5$; third column: $\lambda = 0$.

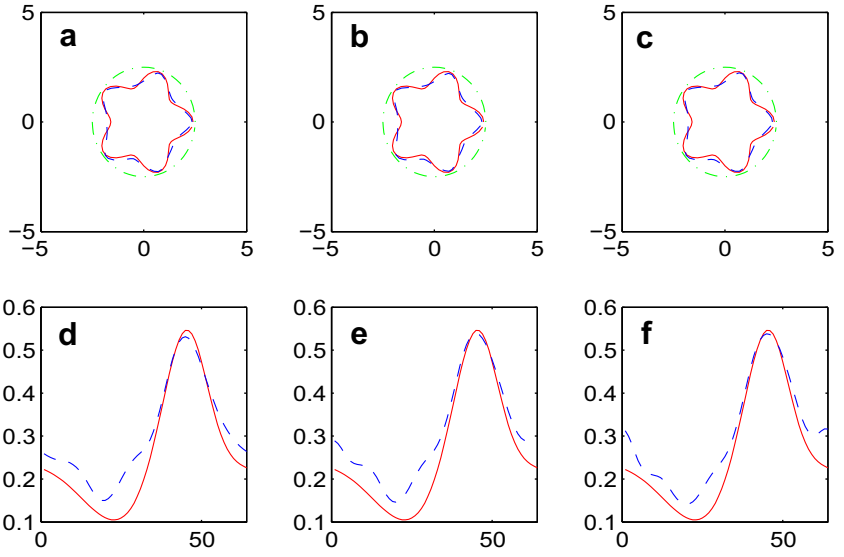

Fig. 4. First row: reconstructions of the shape; second row: reconstructions of the impedance function; first column: two iterations of $\sigma(x)$ per iteration of $\phi(x)$; second column: one iteration of $\sigma(x)$ per two iterations of $\phi(x)$; third column: one iterations of $\sigma(x)$ per four iterations of $\phi(x)$. The initial guess for the impedance function is $\sigma(x) = 1.2$.

function is relatively small compared with the computation time $O(64^3)$ for solving the linear equation (23) by the Gauss–Seidel method.

All of our numerical results shown here, the red solid line denotes the exact shape or the exact impedance function, the green dash dot line denotes the initial shape or the initial impedance function, and the blue dashed line denotes the reconstructed shape or the reconstructed impedance function.

7.1. Reconstruction of ∂D When $\sigma(x)$ is Known

First let us consider a simpler problem. We assume the impedance function $\sigma(x)$ is given and we want to reconstruct the boundary of the obstacle from the given far-field pattern according to the algorithm in Section 4.1.

In Fig. 1 we show our algorithm is stable with respect to the initial guess of the shape. The reconstruction is done on both obstacles, both impedance functions and three different starting shapes: a circle of radius $r = 1.2$, $r = 2.2$ and $r = 3.0$. The

reconstructed results are very good. Particularly for the star shape obstacle, the reconstructions are almost perfect. Moreover, in our numerical experiments we have also noticed that in the case of the star shape with $\sigma(x) = 1$ the range of the initial guess to obtain a good reconstruction is relatively larger compared with the other three cases. The range is from $r_{\min} = 0.4$ to $r_{\max} = 4.1$. But for the leaf shape obstacle, our reconstructed results do not catch all the corners accurately, see Fig. 1(j). One of the reasons is the non-convexity of the leaf shape. In general, the more non-convex of a shape is the harder is to reconstruct the shape, therefore it is harder to reconstruct the leaf shape than the star shape. Moreover, comparing (g) and (j) in Fig. 1, we may conclude that a non-constant surface impedance makes an obstacle more invisible.

7.2. Reconstructions of ∂D and $\sigma(x)$

In Fig. 2 we reconstruct both the star shape and the impedance function $\sigma(x) = 1$ by using different regularization parameters: $\lambda = 1$ shown in the first column, $\lambda = 10$ shown in the second column and $\lambda = 100$ shown in the third column. The initial guesses for the shape and the impedance function are all chosen as $r = 2.5$ and $\sigma(x) = 1.2$. We observe that the reconstructed shapes for three cases are very good with $\lambda = 100$ giving the best reconstruction results, see the third column in Fig. 2.

However, when the surface impedance function is varying instead of constant, it is better to use a smaller regularization parameter. This is tested on the case of the leaf shape and $\sigma(x) = \frac{2+\sin\theta\cos\theta}{(3+\sin\theta)^2}$ with the initial guesses $r = 2.5$ and $\sigma(x) = 0.4$. In Fig. 3, we show the results obtained from $\lambda = 1$, $\lambda = 0.5$ and $\lambda = 0$ in the first column, the second column and the third column respectively. Again we observe that the reconstructed shapes and impedance functions are very good. In particular, in the case of $\lambda = 0$, we are surprised that we are able to reconstruct a shape which matches the exact shape perfectly but with an oscillating impedance function which at least catches the location of the min/max value of the exact impedance function.

As we mentioned, Fig. 4 shows that the reconstructions are not sensitive to the choice of the number of iterations of $\sigma(x)$ per iteration of $\phi(x)$ or vice versa. This is tested on the case of the leaf shape and $\sigma(x) = \frac{2+\sin\theta\cos\theta}{(3+\sin\theta)^2}$ again with the initial guesses $r = 2.5$ and $\sigma(x) = 1.2$ (not shown in Fig. 4 in order to have a closer look of the reconstructed impedance function and the exact impedance function). The regularization parameter $\lambda = 0.5$ for all three cases. Even though the initial impedance function is far away from the exact function the reconstruction results for both the shape and the impedance function are quite good. It indicates that our algorithm is stable with respect to the initial guess for the impedance function as well. We also tested on the same case with an initial impedance function $\sigma(x) = 0.05$, the reconstructed $\sigma(x)$ (not shown here) can still find the peak of the exact $\sigma(x)$ but not the valley of the exact $\sigma(x)$. We are not clear what causes this.

We have also done some experiments to test against "inverse crime" on the case reconstructing both the star shape and the constant impedance function starting from different initial conditions. That is, we first sample on a high number of far-field data by using 128 basis functions. Then with this data we do a linear interpolation to obtain our given far-field data for 64 basis functions. We do obtain similar results compared with an exact data generated from 64 basis functions. Due to space limitations the comparison images are not shown here.

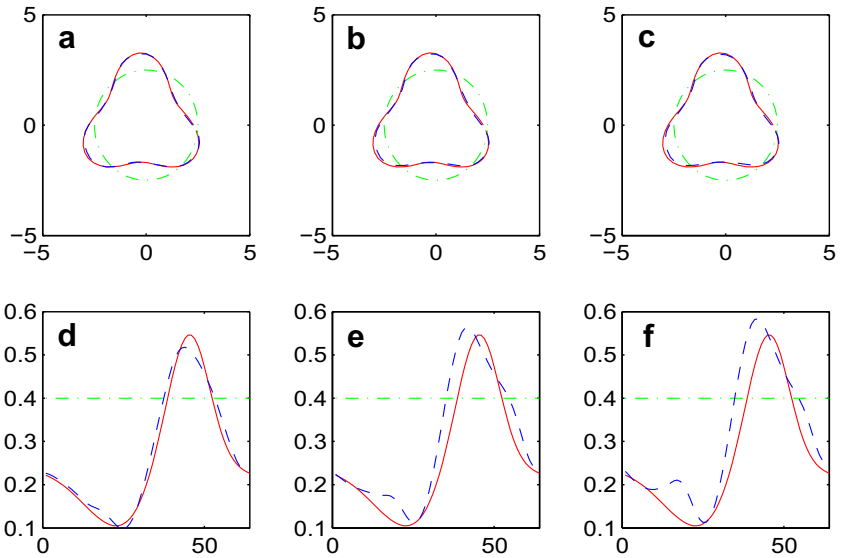

Fig. 5. First row: reconstructions of the shape; second row: reconstructions of the impedance function; first column: noise percentage $\delta = 5\%$, one iteration of $\sigma(x)$ per ten iterations of $\phi(x)$; second column: $\delta = 10\%$, one iteration of $\sigma(x)$ per two iterations of $\phi(x)$; third column: $\delta = 20\%$, one iteration of $\sigma(x)$ per two iterations of $\phi(x)$.

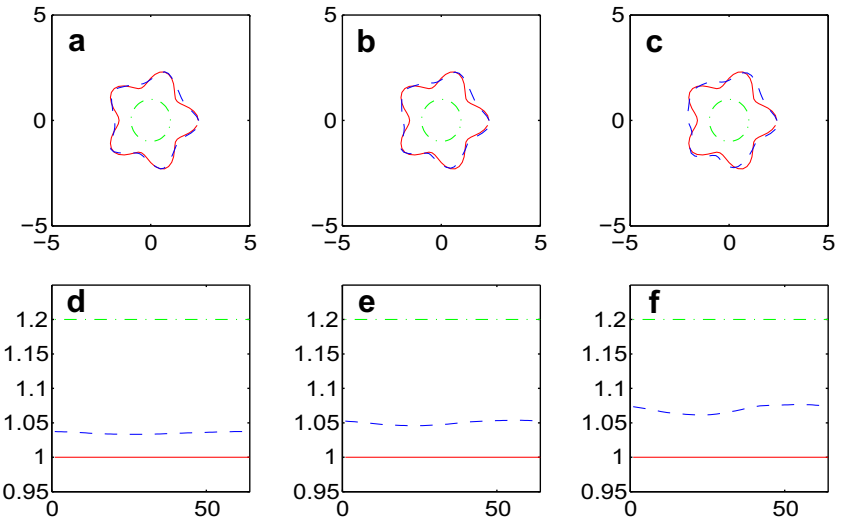

Fig. 6. First row: reconstructions of the shape; second row: reconstructions of the impedance function; first column: noise percentage $\delta = 5\%$, one iteration of $\sigma(x)$ per iteration of $\phi(x)$; second column: $\delta = 10\%$, one iteration of $\sigma(x)$ per iteration of $\phi(x)$; third column: $\delta = 20\%$, one iteration of $\sigma(x)$ per iteration of $\phi(x)$.

7.3. Reconstructions of ∂D and $\sigma(x)$ for noisy data

In this section we reconstruct both the shape and the impedance function of an obstacle from noisy far-field pattern data $g^\delta(\partial D, \sigma)$ with the noise percentage δ defined as

$$\delta := \frac{\|g^\delta - g^0\|_{L^2}}{\|g^0\|_{L^2}},$$

where g^0 is the noise free far-field data obtained from the exact shape D and the exact impedance function $\sigma(x)$.

In Fig. 5 we show the reconstructed results on the star shape obstacle and the varying impedance function from noisy data where $\delta = 5\%$ in the first column, $\delta = 10\%$ in the second column and $\delta = 20\%$ in the third column. All the reconstructions start from the initial guesses $r = 2.5$ and $\sigma(x) = 0.4$. The regularization parameter λ is chosen as 0.5 for all three cases. The results are still good and for the reconstructions from 5% noisy data, the blue dashed line matches the red solid line perfectly for the shape and only a little bit off for the impedance function. Over all the numerical experiments we have observed that the reconstruction for the shape is usually better and more stable than for the impedance function. The third column shows we can still obtain a good shape and a reasonable impedance function even for 20% noise. However, we have to admit that in the noisy cases the initial guess for the shape was very close to the true one. On the other hand, such initial guesses can also be computed rather efficient with sampling/probing type algorithms. So a combination of gradient type methods and sampling type algorithms to obtain initial guesses seems to be quite promising.

Fig. 6 shows the reconstructions on the leaf shape obstacle and the constant impedance function with given noisy data. The noise percentages for the first column, the second column and the third column correspondingly are 5, 10 and 20. All three reconstructions start from the initial guesses $r = 1.0$ and $\sigma(x) = 1.2$. The regularization parameter λ is chosen as 10 this time for all three cases. Here we observe a larger impact of the noise percentage on the reconstructed results, for both the shape and the impedance function.

Acknowledgments

The work of L.H., S.K. and M.S. has been supported by the Austrian National Science Foundation FWF through project SFB F 013/1308 and by the Johann Radon Institute for Computational and Applied Mathematics (Austrian Academy of Sciences ÖAW). The author L.H. wants to thank the director of RICAM Prof. Heinz Engl for his understanding and help with her family issues.

References

[1] G. Alessandrini, L. Rondi, Determining a sound-soft polyhedral scatterer by a single far-field measurement, Proc. Amer. Math. Soc. 133 (6) (2005) 1685–1691. Corrigendum, preprint arXiv math.AP/0601406, 2006 (down-loadable at http://www.arxiv.org/archive/math/).
[2] G. Allaire, F. Jouve, A.-M. Toader, Structural optimization using sensitivity analysis and a level-set method, J. Comput. Phys. 194 (1) (2004) 363–393.
[3] G. Bal, K. Ren, Reconstruction of singular surfaces by shape sensitivity analysis and level set methods, Math. Models Appl. Sci. 16 (2006) 1347–1473.
[4] M. Burger, S. Osher, A survey on level set methods for inverse problems and optimal design, Eur. J. Appl. Math. 16 (2005) 263–301.
[5] Martin Burger, A level set method for inverse problems, Inverse Problems 17 (2001) 1327–1356.

[6] D. Colton, R. Kress, Integral equation methods in scattering theory, Pure and Applied Mathematics (New York), A Wiley-Interscience Publication, New York, 1983.
[7] D. Colton, R. Kress, Inverse Acoustic and Electromagnetic Scattering, Springer, Berlin, 1992.
[8] D. Colton, B.D. Sleeman, Uniqueness theorems for the inverse problem of acoustic scattering, IMA J. Appl. Math. 31 (3) (1983) 253–259.
[9] O. Dorn, D. Lesselier, Level set methods for inverse scattering, Inverse Problems 22 (2006) 67–131.
[10] G.R. Feijoo, A new method in inverse scattering based on the topological derivative, Inverse Problems 20 (2004) 1819–1840.
[11] G.R. Feijoo, A. Oberai, P.M. Pinsky, An application of shape optimization in the solution of inverse acoustic scattering problems, Inverse Problems 20 (2004) 199–228.
[12] D. Gintides, Local uniqueness for the inverse scattering problem in acoustics via the Faber-Krahn inequality, Inverse Problems 21 (4) (2005) 1195–1205.
[13] H. Hesse, Theory and numerics for shape optimization in superconductivity, Ph.D. thesis, Der Mathematisch-Naturwissennschaftlichen Fakultaeten Georg-August-Universitaet zu Goettingen, 2006.
[14] S.M. Hou, K. Solna, H.K. Zhao, A direct imaging algorithm for extended targets, Inverse Problems 22 (2006) 1151–1178.
[15] S.M. Hou, K. Solna, H.K. Zhao, A direct imaging method for far field data, Inverse Problems 23 (2007) 1533–1546.
[16] V. Isakov, Stability estimates for obstacles in inverse scattering, J. Comp. Appl. Math. 42 (1991) 79–89.
[17] V. Isakov, New stability results for soft obstacles in inverse scattering, Inverse Problems 9 (5) (1993) 535–543.
[18] J.B. Keller, D. Givoli, Exact non-reflecting boundary condition, J. Comput. Phys. Spec. 82 (1989) 172–192.
[19] R. Kress, W. Rundell, Inverse scattering for shape and impedance, Inverse Problems 17 (4) (2001) 1075–1085. Special issue to celebrate Pierre Sabatier's 65th birthday (Montpellier, 2000).
[20] J.J. Liu, G. Nakamura, M. Sini, Reconstruction of the shape and surface impedance from acoustic scattering data for arbitrary cylinder, SIAM J. Appl. Math. 67 (2007) 1124–1146.
[21] H. Liu, J. Zou, On unique determination of partially coated polyhedral scatterers with far field measurements, Inverse Problems 23 (1) (2007) 297–308.
[22] F. Murat, S. Simon, Etudes de problems d'optimal design, Lectures Notes in Computer Science 41 (1976) 54–62.
[23] G. Nakamura, M. Sini, Obstacle and boundary determination from scattering data, SIAM J. Math. Anal. 39 (3) (2008) 819–837.
[24] S. Osher, J.A. Sethian, Fronts propagating with curvature dependent speed; algorithms based on Hamilton–Jacobi formulations, J. Comput. Phys. 79 (1988) 12–49.
[25] L. Rondi, Stable determination of sound-soft polyhedral scatterers by a single measurement, Indiana Univ. Math. J. 57 (3) (2008) 1377–1408. Available online at <http://www.iumj.indiana.edu/Preprints/3217.pdf>.
[26] G. Russo, P. Smereka, A remark on computing distance functions, J. Comput. Phys. 163 (2000) 51–67.
[27] F. Santosa, A level-set approach for inverse problems involving obstacles, Control, Optimisation and Calculus of Variations 1 (1996) 17–33.
[28] E. Sincich, M. Sini, Local stability for soft obstacles by a single measurement, Inverse Problems and Imaging 2 (2) (2008) 301–315.
[29] E. Sincich, Stable determination of the surface impedance of an obstacle by far field measurements, SIAM J. Math. Anal. 38 (2) (2006) 434–451.
[30] P. Stefanov, G. Uhlmann, Local uniqueness for the fixed energy fixed angle inverse problem in obstacle scattering, Proc. Amer. Math. Soc. 132 (5) (2004) 1351–1354.
[31] J. Sokolowski, J.P. Zolesio, Introduction to Shape Optimization: Shape Sensitivity Analysis, Springer, Heidelberg, 1992.
[32] A.D. Zacharopoulos, Three-dimensional reconstruction of shape and piecewise constant region values for optical tomography using spherical harmonic parametrization and a boundary element method, Inverse Problems 22 (2006) 1509–1532.